Automatika

Journal for Control, Measurement, Electronics, Computing and Communications

ISSN: (Print) (Online) Journal homepage: https://www.tandfonline.com/loi/taut20

Fast charging converter and control algorithm for solar PV battery and electrical grid integrated electric vehicle charging station

P. Prem, P. Sivaraman, J. S. Sakthi Suriya Raj, M. Jagabar Sathik & Dhafer Almakhles

To cite this article: P. Prem, P. Sivaraman, J. S. Sakthi Suriya Raj, M. Jagabar Sathik & Dhafer Almakhles (2020) Fast charging converter and control algorithm for solar PV battery and electrical grid integrated electric vehicle charging station, Automatika, 61:4, 614-625, DOI: 10.1080/00051144.2020.1810506

To link to this article: https://doi.org/10.1080/00051144.2020.1810506

Published online: 27 Aug 2020.

AUTOMATIKA
2020, VOL. 61, NO. 4, 614–625
https://doi.org/10.1080/00051144.2020.1810506

REGULAR PAPER

OPEN ACCESS Check for updates

Fast charging converter and control algorithm for solar PV battery and electrical grid integrated electric vehicle charging station

P. Prem [a], P. Sivaraman [a], J. S. Sakthi Suriya Raj[a], M. Jagabar Sathik[b,c] and Dhafer Almakhles[c]

[a]Department of Electrical and Electronics Engineering, Bannari Amman Institute of Technology, Sathyamangalam, India; [b]Department of Electrical and Electronics Engineering, SRM Institute of Science and Technology, Chennai, India; [c]Renewable Energy Lab, College of Engineering, Prince Sultan University, Riyadh, Saudi Arabia

ABSTRACT

Electric Vehicles (EV) offer eco-friendly transportation, but the growth of the electric vehicle market year over year is very minimal due to insufficient EV charging stations, slow charging time and grid instability during peak hours. This paper proposes a high gain, fast charging DC–DC converter and a control algorithm for grid integrated Solar PV based Electric Vehicle Charging Station (SPV-EVCS) with battery backup. The proposed converter and its control algorithm's performance are investigated in three different modes using MATLAB/Simulink tool and the simulated results are validated with Real-Time Digital Simulation (RTDS) in OPAL-RT. The observed results meet the Power Quality limits of an IEC61000-3-2 standard and met the level-4 dc charging standard IEC61851.

ARTICLE HISTORY
Received 26 December 2019
Accepted 11 August 2020

KEYWORDS
Fast-Charging; electric vehicle; T-source converter; charging station; grid

1. Introduction

Due to the increase in energy demand and the climate change triggered by CO_2 emission, Electric Vehicle technology has become inevitable in the transportation sector. EV's are classified based on energy source: Battery EVs (BEV), Plug-in hybrid EVs (PHEV) and fuel cell EVs. The fuel cell-based vehicles are limited and under development stage due to the high cost of hydrogen production and risk involved in storage. So, battery EVs and plugged-in hybrid EVs are gaining wide attention [1]. The move from internal combustion engine vehicles to electric vehicle will happen soon and more rapidly than the expectation, but the major barriers for EV commercialization are; size of the battery, time taken to recharge, inefficient power conversion due to multiple stages and grid instability during peak hours due to increased power consumption [2]. A hybrid charging station which is less grid-dependent, can overcome the above barriers. Therefore, SPV-EVCS with a battery backup is now drawing more attention of design engineers and researchers [3].

An SPV-EVCS with battery backup has two types of architecture (1) Common AC bus architecture, (2) Common DC bus architecture and it is represented in Figure 1(a,b) [4,5].

In AC-bus architecture each charging node comprises of a DC–DC charging converter feeding a dedicated DC–AC converter for each source and load, which is then coupled to the AC bus through the high-frequency transformer as shown in Figure 1(a). A common DC-bus architecture requires only one central AC–DC converter, a low-frequency transformer in the grid side and a dedicated DC–DC converter for source and load as shown in Figure 1(b).

DC bus architecture excels AC bus architecture in aspects like simple control circuit and less switching operations resulting in improved stability, reliability and efficiency. Further, AC bus architecture also has synchronization issues [3–5]. The DC bus architecture can be either unipolar or bipolar [6,7]. The unipolar architecture employs conventional two-level converters where in bipolar architecture uses Z-source and multilevel converters. Bipolar converters will be suitable for the implementation of SPV-EVCS as it can facilitate bilateral power exchange between charging station and grid [8]. The selection of converters and control algorithms influences the charging ability of bipolar DC bus architecture. A grid-tied neutral point clamped (NPC) converter for plug-in electric vehicle (PEV) dc fast-charging station is proposed in [9]. The bipolar dc structure of the converter reduces the step-down effort on the dc–dc fast chargers [10]. But, it requires voltage balancing circuits to eliminate the fluctuations in the NPC converter resulting in low current and voltage gain [11]. An NPC converter-based fast charger with voltage balancing coordination for the EV charging station is proposed in [12]. But, unipolar converter cannot be used in SPV-EVCS as it would not facilitate the export of excess power to grid. Also, the dynamic response under the intermittent solar irradiance condition is

CONTACT P. Prem premp@bitsathy.ac.in

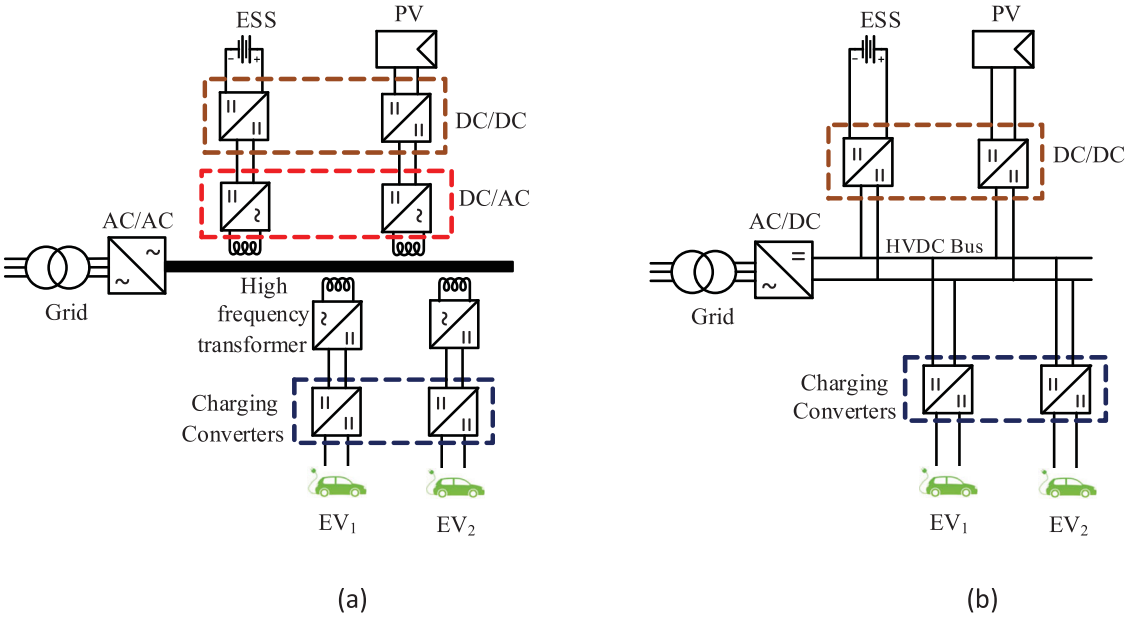

Figure 1. (a) Common AC bus architecture and (b) common DC bus architecture.

poor even though it has more freedom to the grid-side current control and removes the low-frequency ripple in the dc-bus voltages.

A single-stage bidirectional Z-source inverter (ZSI) is designed where the battery is incorporated into the Z-source network thus reducing the cost and improving the performance of the energy storage system [13]. In addition, the DC-bus voltage can be independently controlled by the shoot-through duty cycle, however, it has more ripple in DC-link and the control of dc link voltage is complex. A switched-quasi-Z-source bidirectional dc–dc converter is proposed for electric vehicles (EVs) in [14]. Here, a switched-capacitor cell is connected at high voltage side to achieve a wide range of voltage gain and lower voltage stress across the power switches. But, reliability of the converter is reduced due to the switched capacitor and it also doesn't provide galvanic isolation. A T–source inverter for solar PV grid-connected systems is proposed in [15] and it has the ability to buck–boost the input voltage to the required level and with low input current and output voltage ripples and can solve the above setbacks.

The next side of the EV charger is a bidirectional DC–DC converter for charging stations. A converter with a modular multiport power electronic transformer (M2PET) is presented in [16]. It has high numbers of submodule (split) batteries acting as a power buffer and reduces the influence of the charging station on the distribution grid. However, the control and monitoring of each sub-module are complex. A multiport converter for a smart electric vehicle charging station, with dual/triple active bridge converter, providing multidirectional power flow is proposed. The galvanic isolation is also achieved through a separate high-frequency transformer but, the zero states present in the converter reduces the gain of the converter [17,18]. A multi-input DC–DC Converter is proposed for hybrid electric vehicles and it is operated with fuel cell (FC), photovoltaic (PV) panel and energy storage system (ESS) as the input sources [19]. But the absence of galvanic isolation is a critical factor in this topology. A parallel three-level dc–dc converter with an integrated inductor is proposed for EV fast-charging stations. Though it attenuates the circulating current in the output, the ripple in the output is more due to a higher number of switching operations [20,21]. Solar PV powered three-phase hybrid boost converter is proposed in [22] for the EV charging station. It has a single-stage converter comprising of DC–DC booster and a DC–AC converter, thus resulting in reduced conversion stages and switching loss. Since this converter is connected between PV source and grid without any isolation, it causes galvanic isolation problems and harmonics. A non-isolated bidirectional DC–DC converter developed for hybrid electric vehicle charging, that interfaces dual energy storage, and dc-bus of different voltage levels is presented in [23]. It has uniform current sharing characteristics. However, galvanic isolation and power quality of the converter are not discussed.

Thus, the topologies discussed in the above literature have some common setbacks like (1) lack of bidirectional power flow, (2) reduced gain due to the discontinuous mode of operation (3) slow dynamic response, (4) absence of galvanic isolation in non-isolated converter, (5) high number of semiconductors and passive elements reducing the reliability. Therefore, the T-source inverter which has: (1) reduced power conversion stage with fewer semiconductors and passive elements, (2) high voltage gain and (3) fast dynamic response, is chosen for the proposed DC bus architecture.

In the grid, sudden connection of multiple fast EV chargers may create voltage fluctuation and will lead

to instability in the local grid. Hence control of the converter with dc bus is essential. A Phase-Locked Loop (PLL) based control algorithm for soft switching techniques employed in electric vehicle DC–DC converter is studied in [24], But it requires complex control and is poor in dynamic response. A phase disposition pulse width modulation (PD-PWM) is proposed for a 3-phase 3-level stacked neutral-point-clamped (3L-SNPC) converter to provide zero voltage switching (ZVS) in EV charging system in [25], In this system, the two poles located nearer to the imaginary axis will push the system to unstable state during dynamic input condition. An asymmetric pulse length modulated full-bridge DC–DC converter for ZVS is suggested in [26] and the system has no control over the input intermittency. A sliding-mode controller for DC–DC converter to offer a regulated bus Voltage for safe operation for charging station is dealt in [27]. A Z-source three-level SVPWM inverter with PI controller for Battery charging is proposed [23,28]. Here, the controller has poor transient response and more ripples in the output. A chain of two PI controllers is used in an autonomous energy management system in a residential EV charging point is proposed in [29] and the charging time is high due its sluggish dynamic response. From the above-mentioned control algorithms for EV charging facility, the PI controller has the advantage of zero steady-state error and capability of noise filtering and most widely used in bi-directional power flow control. Hence, modified PWM with a chain of the two-PI controllers is used to achieve the desired DC bus voltage for the proposed bi-directional T-source converter fed EV charging station. The salient features of the converter and the control algorithm proposed are as follows:

(i) T-source impedance network provides high gain with galvanic isolation between array and grid, as well as between grid and the vehicle. This results in improved power quality and voltage stability. This makes the Bidirectional T-Source DC–DC converter suitable for fast charging application.

(ii) the new switching algorithm employed enables the Bidirectional T-Source DC–DC converter to obtain high gain

(iii) The closed loop control algorithm developed using state space averaging technique improves the system's response with reduced current THD. Further it makes the system immune to disturbances.

The paper is organized as follows: literature for DC–DC converter topology for EV charging stations is disclosed and its gaps are identified in Introduction Section 1. The proposed DC–DC converter's operation and its pulse width modulation technique are described in Sections 2–4. Sections 5 and 6 deal with converter optimum parameter selection based on output requirements, dynamic modelling and stability analysis. Section 7 presents the results and discussion and finally concluded in Section 8.

2. System description

Figure 2(a) shows the block diagram of the proposed SPV-EVCS topology. It comprises of a T-shape network interfacing the solar PV and electrical grid, and the T-source DC–DC converter is used for charging EV and the buffer battery. The converters used in this scheme are bi-directional converters as they require two-way power flow when charging and discharging EV and the buffer battery. A bi-directional DC/AC inverter is used to provide grid interfacing that facilitates the supply of surplus power generated by the PV to grid and the consumption of power from grid when demand exists.

3. Proposed T-source DC–DC converter for electric vehicle charging station

The operating modes of the T-source DC–DC converter and its average output voltage are discussed in this section. In order to understand the working of the converter, the converter is supplied with constant input

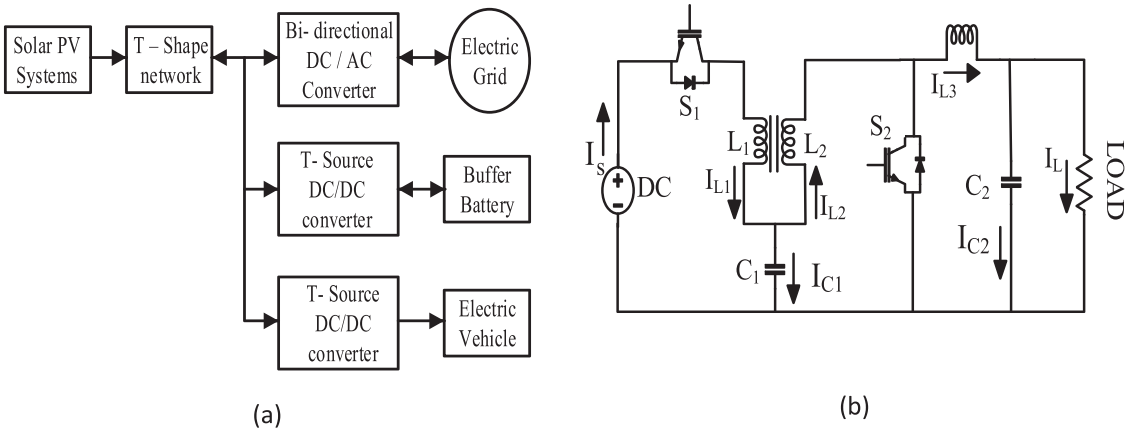

Figure 2. (a) Block diagram of Solar PV, battery backup and electric grid integrated EV-charging station and (b) circuit diagram of T source DC–DC converter.

voltage and its terminals are connected to a resistive load.

T-source DC–DC converter consists of a pair of mutually coupled inductors L_1 and L_2 and a capacitor (C_1) connected in T-shape to the input DC bus as shown in Figure 2(b). This converter can produce the desired output DC voltage irrespective of the input voltage fluctuations due to the intermittent nature of solar power. The T-source DC–DC converter has two operating modes, namely non-shoot-through mode and shoot-through mode based on the switching states of switches S_1 and S_2 [10].

In non- shoot-through mode, the switch S_1 is ON and S_2 is OFF. Figure 3(a) shows the equivalent circuit of TSI in non-shoot through mode. During this time energy is transferred from source to load, and the output voltage is based on the duty ratio of switch S_1. Further, the input capacitor C_1 is charged with the input current I_1 and the output inductor L_3 is energized. In shoot-through mode both switch S_2 and switch S_1 are turned ON as shown in Figure 3(b). Thus, the charge stored in capacitors C_1 and C_2 is transferred to inductors L_2 and L_3 respectively. The total voltage across the T-network is based on the number of turns in inductor L_2. The inductor L_2 and capacitor C_1 are now forming a parallel connection as shown in Figure 3(b). Assuming the inductors in the T-network are identical (i.e. $L_1 = L_2 = L_T$). The voltage across the inductors and capacitors can be expressed as

$$V_{C1} = V_{C2} = V_C \tag{1}$$

$$V_{L1} = V_{L2} = V_L \tag{2}$$

When the converter is in non-shoot through operation as shown in Figure 3(a), for a duration T_{non}, the inductor voltage (V_L) voltage across the switch S_2 (V_d) and the source voltage (V_S) can be written as

$$V_{L1} = V_S - V_{C1} \tag{3}$$

$$V_d = V_{C1} - V_{L2} = 2V_{C1} - V_S \tag{4}$$

When the converter is in shoot-through operation for a duration T_S, the voltage across the diode, inductor L_2 and capacitor C_1 can be written as

$$V_d = 0 \tag{5}$$

$$V_{L2} = V_{C1} \tag{6}$$

The total switching time is $T = T_{non} + T_s$. The capacitor voltage (V_{C1}) can be obtained by equating the average of the inductor voltage over one switching cycle T as zero and can be derived as

$$V_{C1} = \left(\frac{T_{non}}{T_{non} - T_s}\right) V_s = \left(\frac{1-D}{1-2D}\right) V_S \tag{7}$$

If the turns ratio of the mutually coupled coil is 1: n, then the output voltage will be

$$V_{om} = \frac{1}{T}\int_0^T V_d(t)dt = \frac{T_s.0 + T_n(2V_{CZ} - V_S)}{T} \tag{8}$$

The output voltage and the duty cycle can be related as

$$V_{oD} = \left(\frac{T_n}{T_n - T_s}\right) V_s = \left(\frac{1-nD}{1-D(n+1)}\right) V_S \tag{9}$$

where $D = T_s/T$ is the shoot-through duty cycle.

4. Modulation and switching algorithm

In order to enhance the charging rate of converter a modified pulse width modulation scheme is proposed for the T source DC–DC converter and it is presented in Figure 4.

From Figure 4, it can be observed that S_1 and S_2 are ON when V_{GS1} is high and S_2 is ON when V_{GS2} is high and the shoot through pulse turns ON both S_1 and S_2 (Table 1). During the shoot through period, energy is transferred from capacitor to inductor. After the shoot-through period inductor energy is transferred to the battery along with input energy supplied by the source. The shoot-through time (T_{sh}) is calculated based on capacitor and inductor energy storage value.

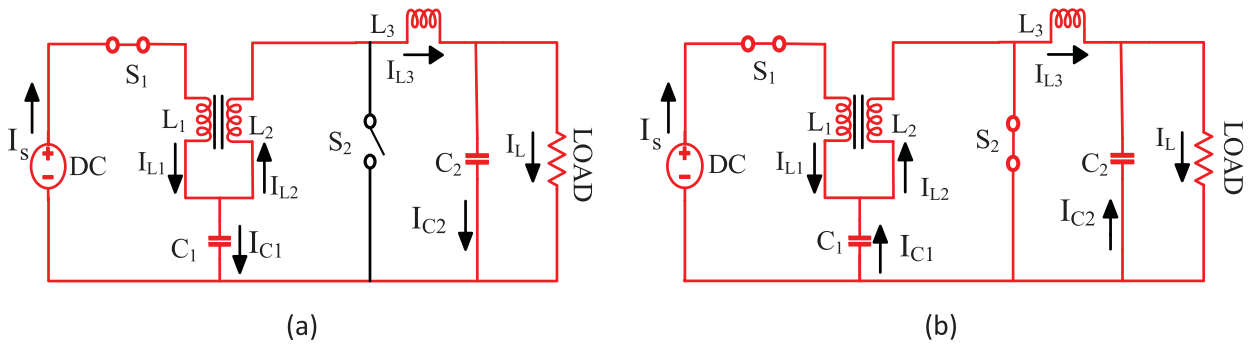

Figure 3. Operation of T- source DC–DC converter in (a) non-shoot through mode and (b) shoot-through mode.

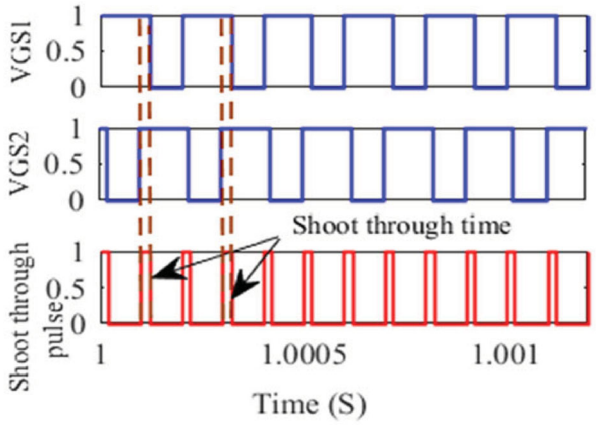

Figure 4. Pulse width modulation scheme of T Source DC–DC converter.

Table 1. Pulse modulation algorithm.

Pulse width	Time (s)	VGS_1	VGS_2
0–10	1.00002	**High**	**High**
10–20	1.00004	High	Low
20–30	1.00006	High	Low
30–40	1.00008	High	Low
40–50	1.00010	High	Low
50–60	1.00012	**High**	**High**
60–70	1.00014	Low	High
70–80	1.00016	Low	High
80–90	1.00018	Low	High
90–100	1.00020	Low	High

5. Effect of inductance and duty cycle variation

The charging current rate is influenced by the inductance of the T-source impedance network. The inductance of the T-source impedance network is varied from 0.01 to 20 mH and the corresponding charging currents are measured using the simulation model and plotted as shown in Figure 5(a,b). As per IEC 61851 maximum current of dc level-3 charger is 400 A with maximum dc voltage up to 600 V. Therefore, inductor values $L_1 = L_2 = 5$ mH is chosen as the optimum value so that the maximum current of 378 A can be obtained during charging.

The duty cycle of the proposed DC–DC converter is varied from 0.1 to 0.9 with a shoot-through time of 0.15 ms and its corresponding charging current is recorded as shown in Figure 5(b). As per IEC 61851 maximum, the allowable charging current is 400 A. From Figure 5(b), it is observed that at a duty cycle of 0.48 to 0.58 the charging current is greater than standard value and at 0.6 duty cycle charging current is 378 A and hence the duty cycle 0.6 is chosen as optimum value.

6. Dynamic modelling of T source DC–DC converter

The power supplied by the solar PV plant to the charging station will vary due to the intermittent irradiance and load profile of the charging station and hence study of dynamic behaviour of proposed T source DC–DC converter under fast-changing environment is necessary. In this section dynamic model of T source DC–DC converter is developed using state-space technique and its stability is analysed under the open-loop and closed-loop conditions with a proportional–integral controller used in the closed-loop. The coupled inductor current (i_L), T-source capacitor voltage (V_c), converter inductor current (I_0) and converter capacitor voltage (V_{co}) are the state variables represented in Equation (11).

$$x(t) = [i_L(t), V_c(t), I_o(t), V_{Co}(t)] \tag{11}$$

From Figure 3(a,b), state equation of shoot through and non-shoot through modes are obtained and it is represented in Equations (12) and (14)

$$K\frac{dx(t)}{dt} = A_1x(t) + B_1u(t) \tag{12}$$

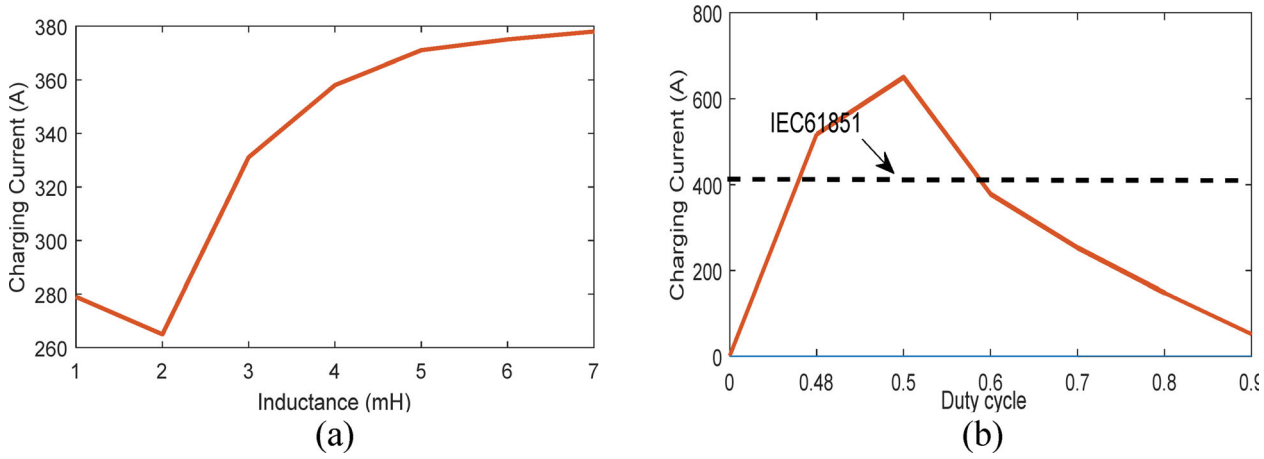

Figure 5. Effect of charging current due to (a) inductance variation and (b) duty cycle variation.

$$\begin{bmatrix} L & 0 & 0 & 0 \\ 0 & C & 0 & 0 \\ 0 & 0 & L_o & 0 \\ 0 & 0 & 0 & C_o \end{bmatrix} \frac{d}{dt} \begin{bmatrix} I_L \\ V_C \\ I_{L_o} \\ V_{C_0} \end{bmatrix} = \begin{bmatrix} 0 & 1 & 0 & 0 \\ -1 & 0 & 0 & 0 \\ 0 & 0 & 0 & -1 \\ 0 & 0 & 1 & -\frac{1}{R_L} \end{bmatrix} \begin{bmatrix} I_L(t) \\ V_C(t) \\ I_{L_o}(t) \\ V_{C_0}(t) \end{bmatrix} + \begin{bmatrix} 0 \\ 0 \\ 0 \\ 0 \end{bmatrix} [V_s(t)] \tag{13}$$

where

$$K = \begin{bmatrix} L & 0 & 0 & 0 \\ 0 & C & 0 & 0 \\ 0 & 0 & L_o & 0 \\ 0 & 0 & 0 & C_o \end{bmatrix} A_1 = \begin{bmatrix} 0 & 1 & 0 & 0 \\ -1 & 0 & 0 & 0 \\ 0 & 0 & 0 & -1 \\ 0 & 0 & 1 & -\frac{1}{R_L} \end{bmatrix}$$

$$B_1 = \begin{bmatrix} 0 \\ 0 \\ 0 \\ 0 \end{bmatrix}$$

For non -shoot through

$$K\frac{dx(t)}{dt} = A_2x(t) + B_2u(t) \tag{14}$$

$$\begin{bmatrix} L & 0 & 0 & 0 \\ 0 & C & 0 & 0 \\ 0 & 0 & L_o & 0 \\ 0 & 00 & C_o & \end{bmatrix} \frac{d}{dt} \begin{bmatrix} I_L(t) \\ V_C(t) \\ I_{L_o}(t) \\ V_{C_0}(t) \end{bmatrix} = \begin{bmatrix} 0 & -1 & 0 & 0 \\ 1 & 0 & -1 & 0 \\ 0 & 2 & 0 & -1 \\ 0 & 0 & 1 & -\frac{1}{R_L} \end{bmatrix} \begin{bmatrix} I_L(t) \\ V_C(t) \\ I_{L_o}(t) \\ V_{C_0}(t) \end{bmatrix} + \begin{bmatrix} 1 \\ 0 \\ -1 \\ 0 \end{bmatrix} [V_s(t)] \tag{15}$$

where

$$K = \begin{bmatrix} L & 0 & 0 & 0 \\ 0 & C & 0 & 0 \\ 0 & 0 & L_o & 0 \\ 0 & 0 & 0 & C_o \end{bmatrix} A_2 = \begin{bmatrix} 0 & -1 & 0 & 0 \\ 1 & 0 & -1 & 0 \\ 0 & 2 & 0 & -1 \\ 0 & 0 & 1 & -\frac{1}{R_L} \end{bmatrix}$$

$$B_2 = \begin{bmatrix} 1 \\ 0 \\ -1 \\ 0 \end{bmatrix}$$

Comparing Equations (12) and (14)

$$K\frac{dx(t)}{dt} = (DA_1 + (1-d)A_2)\dot{x}(t) + (DB_1 + (1-D)B_2\hat{U}(t) + (A_1 - A_2)X + (B_1 - B_2)U)d(t) \tag{16}$$

The small-signal model equation of the T-source DC–DC converter is obtained by taking the Laplace transform of Equation (16) and it is represented in Equations (18)–(20).

$$SL_oI_o(s) = (2-2D)V_C(s) - (V_{Co}(s) + (D-1)V_s(s) - (-2V_C - V_s)\hat{d}(s) \tag{17}$$

$$SL_1I_1(s) = (2D-1)\widehat{V}_c(s) + (1-D)\widehat{V}_s(s) + (2V_C - V_s)\hat{d}(s) \tag{18}$$

$$SCV_C(s) = (1-2D)I_L(s) + (I_{lo} - 2I_L)\hat{d}(s) + (D-1)I_o(s) \tag{19}$$

$$SC_oV_{Co}(s) = IL_o(s) - \frac{V_{Co}(s)}{R_L} \tag{20}$$

$$SI_o(t) = (2-2D)I_L(s) + (D-1)I_{Lo}(S) + (I_{Lo} - 2I_L)\hat{d}(s) \tag{21}$$

The small-signal equation of converter capacitor voltage is expressed in Equation (22)

$$V_{C0}(s) = \hat{d}(s)GV_{cd}(s) + V_s(s)GV_g(s) \tag{22}$$

From Equation (22), duty ratio control to capacitor voltage is obtained and it is represented in Equation (23)

$$G_{Vd}(s) = \frac{V_{co}(s)}{\hat{d}(s)}|_{V(s)\to 0} = \frac{V_o(s)}{\hat{d}(s)}|_{Vs(s)=0} \tag{23}$$

The converter is designed using specifications listed in Table 2 and its stability is analysed with control to capacitor voltage transfer function $G_{Vd}(s)$ in the frequency domain and results are shown in Figure 6.

The frequency response of controller less T-Source DC–DC converter's transfer function is shown in Figure 6(a). From the figure it can be observed that the gain margin is infinity and the phase margin is 70°. This makes the system unstable resulting in increased settling time and ripples in the output. In order to stabilise the system a control loop with a chain of two PI controllers is proposed which is shown in Figure 7. The outer voltage control loop regulates the voltage and the inner loop ensures a ripple free charging current. The frequency response of the T-Source DC–DC converter with this chain of controllers is shown in Figure 6(b). From the figure it can be found that the gain margin

Table 2. Converter specification.

Converter component	Specification
Input voltage (V_s)	200 V
Output voltage (V_o)	48 V
Switching frequency	2 kHz
Coupled inductor ratio	1:n
Coupled inductor $L_1 = L_2$	5 mH
T-source capacitor C	300 μF
Converter capacitance C_0	220 μF

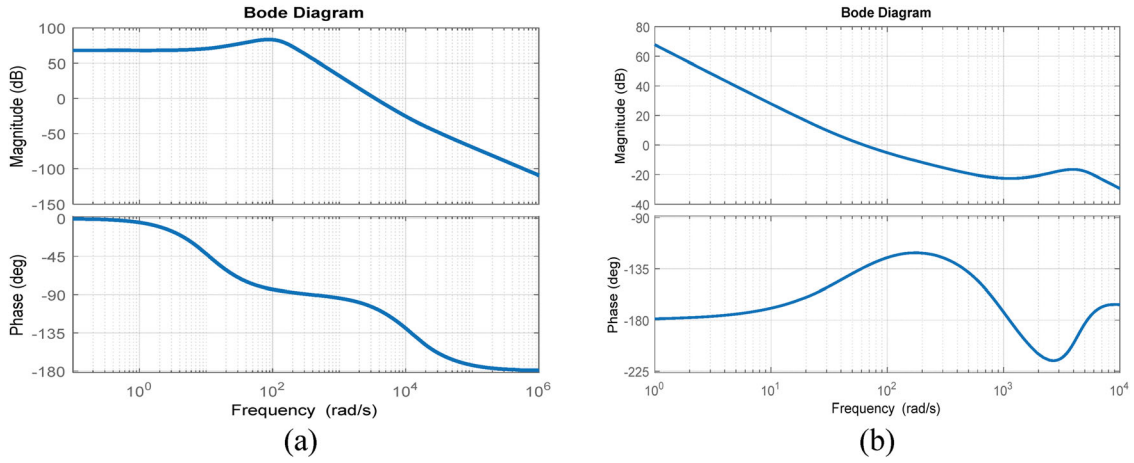

Figure 6. Frequency response of $G_{vcd}(s)$. (a) Open-loop bode plot and (b) closed-loop bode plot with PI controller.

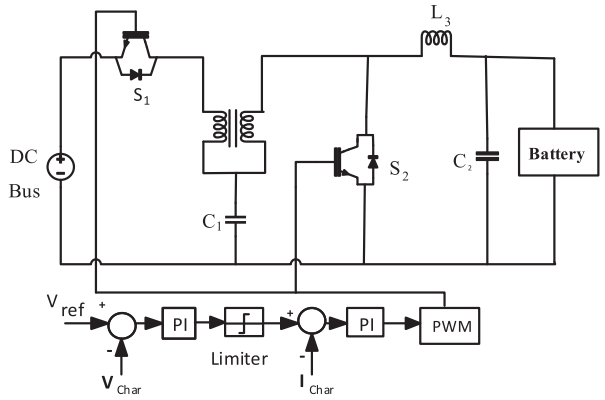

Figure 7. The closed-loop control algorithm for a DC–DC converter with a PI controller.

Table 3. Design specification of the DC–DC converter charging station.

Component	Specification
Grid supply	1ϕ, 230 V, 50 Hz AC
PV plant	20 kWp
Buffer battery	4 Nos. each of 48 V, 100 Ah
Power	15 kW
Output voltage	48 V
Output DC current, *I* Max	400 A
Switching frequency, fs	2 kHz
Coupled inductor,	5 mH
Capacitor, $C_1 = C_2$	300 µF

is 3.3 dB and the phase margin is 56°, thus improving the system stability and reduces the settling time and current ripples.

7. Result and discussion

The suggested system is designed and simulated with parameters given in Table 3. The performance of the given system is investigated with three different modes, namely stand-alone solar-powered electric vehicle charging mode (SPV-EV), Buffer battery to vehicle charging mode (Bb-EV), and Grid to vehicle charging mode (G-EV). In grid-connected mode; a single-phase supply voltage of 230 V, 50 Hz is considered as grid voltage and the dc-link voltage of the bidirectional converter is maintained at 400 V. The proposed converter performance is simulated using MATLAB and the results are validated with Real-Time Digital Simulation (RTDS) in OPAL-RT in three different modes.

7.1. Solar PV to vehicle (SPV-EV) charging mode

In the daytime, power from solar PV plant (P_{PV}) is greater than or equal to the demand created by the vehicle charging requirements thus, the charging station is operated in SPV to EV charging mode. In this mode, EVs are charged with a Solar PV system connected to the charging station.

The PV plant voltage (V_{PV}), current (I_{PV}), battery voltage (V_b), battery charging current (I_b) and state of charge (SoC) of battery are represented in Figure 8(a) from top to bottom respectively. From the waveforms it can be observed that the solar PV plant average output voltage (V_{pv}) is 200 V, output current (I_{PV}) is 250 A with a maximum power rating of 50 kW solar PV system. The battery charging voltage is 52 V, with a charging current of 380 A and initial State of Charge (SOC) of battery at 80% and the battery SoC reaches 80.04% in 1.5 s and hence 12.5 min is required to completely charge the battery SoC of 100%. In this case, solar PV plant is generating required DC power and it is linked to dc bus, the EV chargers are connected to DC bus and they take power directly through the bi-directional T source DC–DC converter to charge the vehicles. In this mode, the DC–DC converter is operated as a buck converter. The excess power from the PV plant is fed to charge the storage battery (buffer) and further excess power could be exported to the local grid. The stored energy from the buffer battery is utilized during insufficient power generated from the SPV unit to charge the EVs.

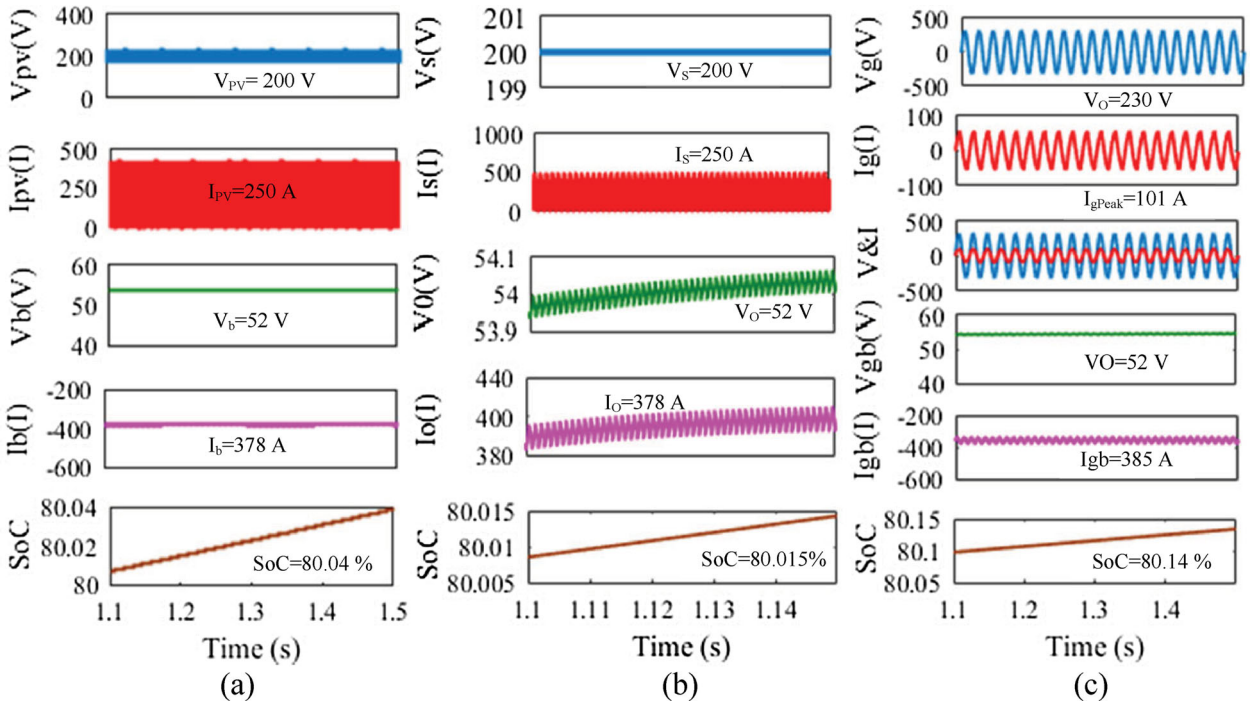

Figure 8. Simulation results of EV charger during: (a) SPV-EV mode, (b) Bb-EV mode and (c) G-EV mode.

7.2. Buffer battery to vehicle (Bb-EV) charging mode

The charging station continues to charge the vehicles connected at the station using the buffer battery (Mode 2 operation), during the absence of the solar PV generation. The performance of the EV charging converter via buffer battery is illustrated in Figure 8(b). The battery voltage (V_S), current (I_S), load voltage (V_0), load current (I_0) and state of charge of battery (SoC) are represented in Figure 8(b) from top to bottom respectively. In these waveforms, the average output voltage (V_S) of SPV unit is 200 V, output current (I_S) of 250 A with a maximum power rating of 50 kW as shown in Figure 8(b). The buffer battery voltage (V_0) is 52 V, the average charging current (I_0) of 380 A and initial State of Charge (SoC) of battery is 80% and it reaches 80.015% in 1.15 s. In this case, EVs are charged slower when compared to mode 1 operation. The corresponding experimental results are represented in Figure 8(b). The power delivered by the buffer battery is pure DC as shown in Figure 8(b) (i) and is used to charge the vehicle in the absence of PV. Figure 8(b) (ii) shows the EV battery charging voltage current and its state of charge respectively.

7.3. Grid to vehicle (G-EV) charging mode

When the power generation using Solar PV is not available and when the buffer battery doesn't carry enough charge to meet the demand, power is drawn from the grid to charge EV. The grid is used to charge the EV directly where the T source bidirectional inverter acts as a rectifier that converts the AC power to DC power. Since the EV is charged directly from the grid without charging the buffer battery the power drawn from the grid is less. The simulation result of the grid voltage (V_g), grid current (I_g), grid to battery charging voltage (V_{gb}), grid to battery charging current (I_{gb}) and state of charge (SoC) during grid to vehicle mode is shown in Figure 8(c). A single-phase $V_{g\text{RMS}}$ of 230 V 50 Hz grid supply is used to charge the EV, the current drawn from the grid is $I_{g\text{RMS}}$ is 101 A given to the T-source converter and used to charge the 48 V battery using T-source converter. The battery charging voltage V_{gb} is of 54 V, and charging current I_{gc} is 385 A. The simulated result shows that within 1.5 s the percentage of SoC increase from 80% to 80.14% thus it requires only 15 min to charge the battery from 0 to 80%. In this mode, the charging station draws power from the grid at unity power factor (UPF) even when the EV is drawing non-sinusoidal current as shown in Figure 8(c). The experimental results of the grid to Electric vehicle are shown in Figure 9(c). Figure 9(c) (i) shows the grid voltage and current which is the input to the AC–DC converter and used to feed the EV. There is no phase lag between the source current and source voltage as can be seen from Figure 9(c). Figure 9(c) (ii) shows the EV charging voltage, current, and state of charge. The power fed from the grid to EV is pure DC with less ripple. Figure 10 shows the THD of the grid current as 3.4% which is under the limits of the IEEE-519 standard. The impedance source network acts a filter. The inductance of the T-source DC–DC converter filters the non-linearity induced by the converters employed in the source side from propagating to the load. This reduces the input current THD of the load.

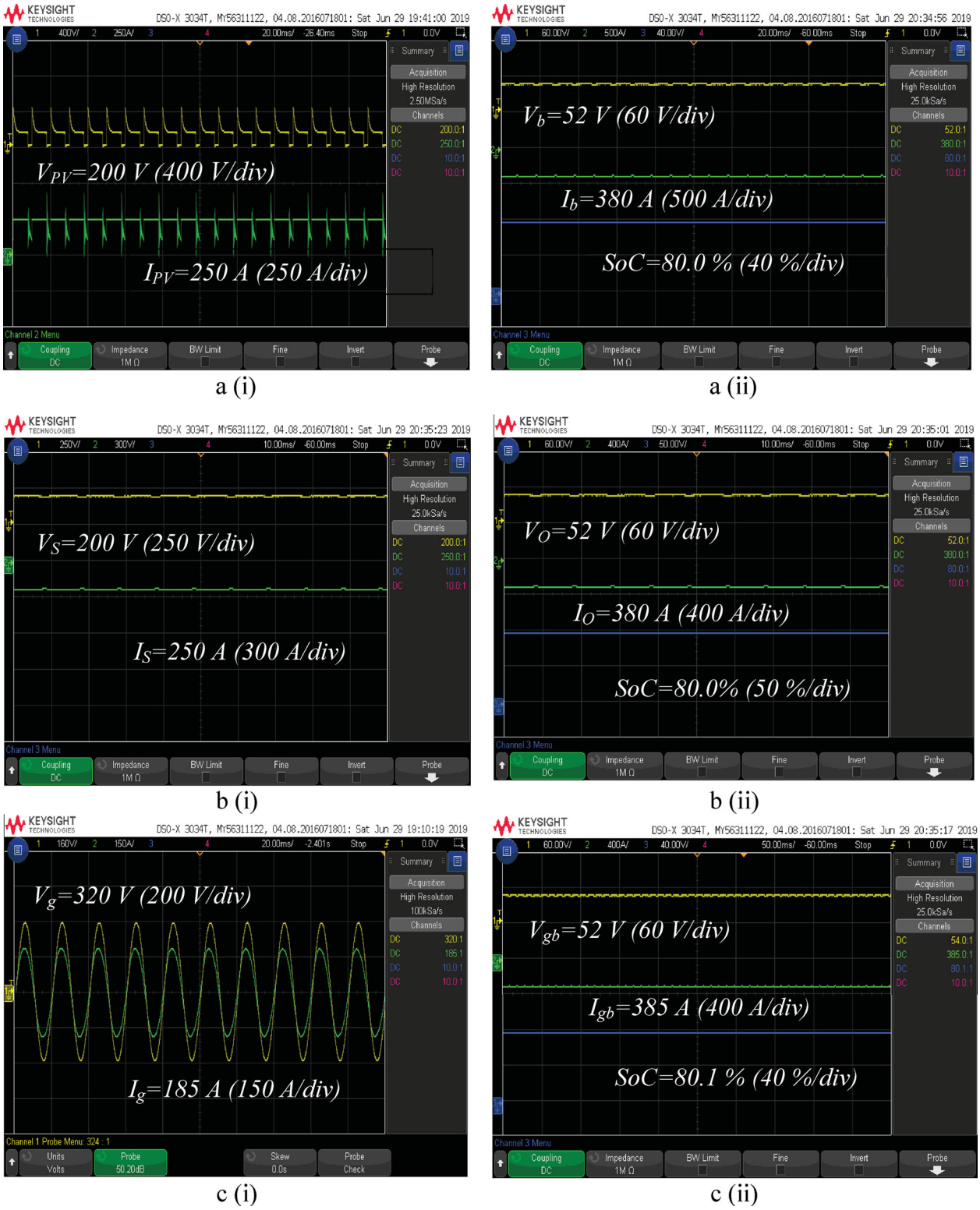

Figure 9. Hardware results of (i) Input voltage and input current (ii) Converter charging voltage, current, and state of charge EV charger during: (a) SPV-EV mode, (b) Bb-EV mode and (c) G-EV mode.

7.4. Dynamic response of the T-source DC–DC converter

Both the source and load of the EV charging stations are fluctuating since the vehicle connected to the charging station keeps on connecting/disconnecting. Therefore, it is necessary to evaluate the dynamic performance of the proposed charging T source converter under dynamic source and load conditions. From Figure 11(a), it can be observed that the charging current from the T-source DC–DC converter is nearly 8% higher when compared to the conventional buck converter. This higher charging current is due to the higher gain offered by the impedance network of the former. The higher charging current reduces the charging time

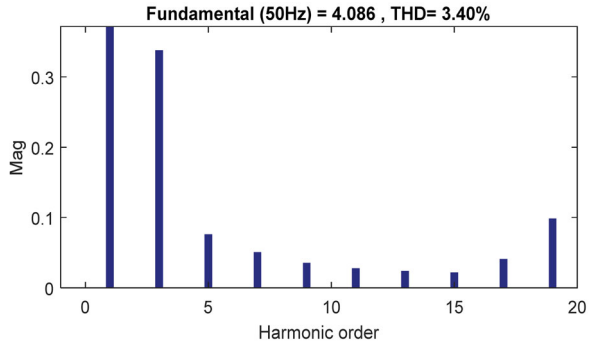

Figure 10. Input current harmonics spectrum during grid to vehicle charging mode.

of the T-Source DC–DC converter-based architecture when compare to other topologies as depicted in Table 4. The plot of charging voltage against time shown in Figure 11(b) indicates that the charging voltage of the T-Source DC–DC converter is slightly higher than the conventional buck converter with relatively less ripple. This reduces the switching stress of the T-Source DC–DC converter when compared to other topologies. The charging current, charging voltage, and the response of conventional buck converter and T source dc–dc converter under step change in irradiance 800 to 1000 w/m^2 are portrayed in Figure 11(c).

From the figure it can be found that during step change in irradiance at 1.5 s the T-Source DC–DC converter undergoes smooth transition between the stable states. Thus, the overshoot of the T-Source DC–DC converter is comparatively low when compared to other topologies also presented in Table 4. The system is subjected to change in irradiance at 1.5 s as shown in Figure 11(c). The response time of the dc–dc converter is 50 ms

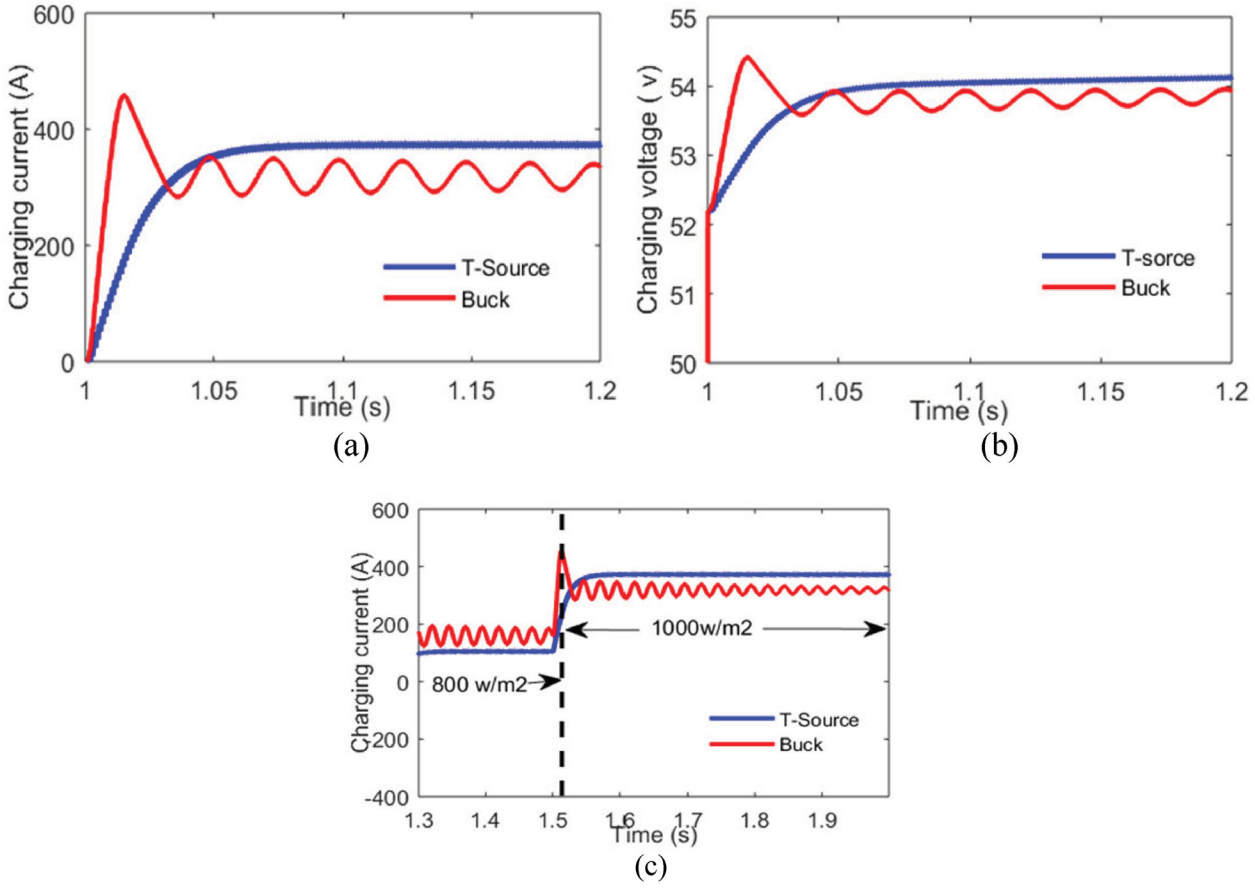

Figure 11. Dynamic response of T-source DC–DC converter (a) charging current of TSC and BC, (b)charging voltage of TSC and BC and (c) step change in PV irradiance.

Table 4. Comparison of T-source DC–DC Converter with other topologies.

Parameter	Conventional buck converter	Interleaved boost converter	Z-source DC–DC converter	T-Source DC–DC Converter
Gain	Very Low	Maximum 2	High	Very high
Input current THD	8.3%	7.2%	5.8%	3.4%
Dynamic response	250 ms	> 250 ms	100 ms	50 ms
Current ripple	12.5%	12.5%	< 2.5%	< 2.5%
Rise time	1.02 s	1.08 s	2.02 s	1.05 s
Overshoot	high	Very high	Low	Very low
Switching current stress	80 A higher than normal value for 50 ms	high	low	Very low
Charging time (80% charging)	Charging time is high due to low gain property	Charging time is very high	medium	Charging time is low due to high current gain.

and the buck converter's response time is 250 ms which is 5 times that of the former. Also, the rise time of buck converter is 1.02 s and it is 3% lesser when compared to T- source DC–DC converter, the lower rise time of the buck converter results in high inrush current. The high inrush current increases the battery's cell temperature and also inflicts damage to the semiconductor switches. The high current gain and low ripple are achieved through the control of operating states of the converter using the modified PWM and the chain of two PI controllers. The efficient design of closed loop PI controller contributed to the improved response and less overshoot. The higher rise time will result in increased life of battery and switches.

8. Conclusion

The proposed T-source DC–DC converter has been found to be an ideal choice for EV fast-charging stations. T-source converter with a battery provides constant current/ constant voltage mode control using its shoot through operation and it also has other advantages like reduced power components, low THD, low ripple, high gain and swift charging. A solar EV grid-connected charging topology is designed and simulated using MATLAB/Simulink tool. simulation results verify the performance of the converter's operation for rated specifications as well as for certain disturbances in rated supply. The overall performance of the proposed converter is found to be satisfactory with low input current THD according to the international IEC 61000-3-2 PQ standard.

Disclosure statement

No potential conflict of interest was reported by the author(s).

ORCID

P. Prem http://orcid.org/0000-0003-0492-0472
P. Sivaraman http://orcid.org/0000-0003-0577-8420

References

[1] Chandra Mouli GR, Kefayati M, Baldick R, et al. Integrated PV charging of EV fleet based on energy prices, V2G, and offer of reserves. IEEE Trans Smart Grid. Mar 2019;10(2):1313–1325. DOI:10.1109/TSG.2017.2763683.
[2] Gjelaj M, Hashemi S, Traeholt C, et al. Grid integration of DC fast-charging stations for EVs by using modular Li-ion batteries. IET Gener Transm Distrib. 2018;12(20):4368–4376.
[3] Khan W, Ahmad F, Alam MS. Fast EV charging station integration with grid ensuring optimal and quality power exchange. Eng Sci Technol Int J. 2019;22(1):143–152. DOI:10.1016/j.jestch.2018.08.005.
[4] Bai S, Lukic SM. Unified active filter and energy storage system for an MW electric vehicle charging station. IEEE Trans Power Electron. 2013;28:5793–5803.
[5] Rivera S, Wu B, Jiacheng W, et al. Electric vehicle charging station using a neutral point clamped converter with bipolar DC bus and voltage balancing circuit. Proceedings of the IECON 2013 – 39th Annual Conference of the IEEE Industrial Electronics Society; 2013 Nov 10–13; Vienna, Austria, p. 6219–6226.
[6] Bai S, Lukic S. Design considerations for DC charging station for plug-in vehicles. Proceedings of the 2011 IEEE Vehicle Power and Propulsion Conference; 2011 Sep 6–9; Chicago, IL, USA; p. 1–6.141.
[7] Kwasinski A. Quantitative evaluation of DC microgrids availability: effects of system architecture and converter topology design choices. IEEE Trans Power Electron. 2011;26:835–851.
[8] Singh SA, Carli G, Azeez NA, et al. Modeling, design, control, and implementation of a modified Z-source integrated PV/grid/EV DC charger/inverter. IEEE Trans Ind Electron. Jun 2018;65(6):5213–5220.
[9] Rivera S, Wu B, Kouro S, et al. Electric vehicle charging station using a neutral point clamped converter with bipolar DC Bus. IEEE Trans Ind Electron. Apr 2015;62(4):1999–2009. DOI:10.1109/TIE.2014.2348937.
[10] Haubert T, Mindl P, Čeřovský Z. Design of control and switching frequency optimization of DC/DC power converter for super-capacitor. Automatika. 2016;57(1):141–149.
[11] Tan L, Wu B, Rivera S, et al. Comprehensive DC power balance management in high-power three-level DC-DC converter for electric vehicle fast charging. IEEE Trans Power Electron. Jan 2016;31(1):89–100. DOI:10.1109/TPEL.2015.2397453.
[12] Tan L, Wu B, Yaramasu V, et al. Effective voltage balance control for bipolar-DC-bus-fed EV charging station with three-level DC-DC fast charger. IEEE Trans Ind Electron. Jul 2016;63(7):4031–4041. DOI:10.1109/TIE.2016.2539248.
[13] Choobdari Omran K, Mosallanejad A. SMES/battery hybrid energy storage system based on bidirectional Z-source inverter for electric vehicles. IET Electr Syst Transp. 2018;8(4):215–220. DOI:10.1049/iet-est.2017.0100.
[14] Zhang Y, Liu Q, Gao Y, et al. Hybrid switched-capacitor/switched-quasi-Z-source bidirectional DC–DC converter with a wide voltage gain range for hybrid energy sources EVs. IEEE Trans Ind Electron. Apr 2019;66(4):2680–2690.
[15] Sivaraman P, Prem P. PR controller design and stability analysis of single stage T-source inverter based solar PV system. J Chin Inst Eng. Apr 2017;40(3):235–245.
[16] Vasiladiotis M, Rufer A. A modular multiport power electronic transformer with integrated split battery energy storage for Versatile ultrafast EV charging stations. IEEE Trans Ind Electron. May 2015;62(5):3213–3222. DOI: 10.1109/TIE.2014.2367237.
[17] Khan SA, Islam MR, Guo Y, et al. A New isolated multi-Port converter With multi-directional power flow capabilities for smart electric vehicle charging stations. IEEE Trans Appl Supercond. Mar 2019;29(2):1–4. DOI:10.1109/TASC.2019.2895526. Art no. 0602504.
[18] Devi Vidhya S, Balaji M. Hybrid fuzzy PI controlled multi-input DC/DC converter for electric vehicle application. Automatika. 2020;61(1):79–91.
[19] Ahrabi RR, Ardi H, Elmi M, et al. A novel step-up multiinput DC-DC converter for hybrid electric vehicles application. IEEE Trans Power Electron.

May 2017;32(5):3549–3561. DOI:10.1109/TPEL.2016.2585044.

[20] Tan L, Zhu N, Wu B. An integrated inductor for Eliminating circulating current of parallel three-level DC-DC converter-based EV fast charger. IEEE Trans Ind Electron. Mar 2016;63(3):1362–1371. DOI:10.1109/TIE.2015.2496904.

[21] Prabhakar S, Febin Daya JL. A comparative study on the performance of interleaved converters for EV battery charging, 2016 IEEE 6th International Conference on Power Systems (ICPS), New Delhi, 2016, p. 1–6.

[22] Tazay A, Miao Z. Control of a three-phase hybrid converter for a PV charging station. IEEE Trans Energy Convers. Sep 2018;33(3):1002–1014. doi:10.1109/TEC.2018.2812181.

[23] Lai C, Cheng Y, Hsieh M, et al. Development of a bidirectional DC/DC converter with dual-battery energy storage for hybrid electric vehicle system. IEEE Trans Veh Technol. Feb 2018;67(2):1036–1052. DOI:10.1109/TVT.2017.2763157.

[24] Reis F, Bascope P, Tofoli F. (2018). Bidirectional three-phase 3L-SNPC converter for EV charging stations. 2018 13th IEEE International Conference on Industry Applications (INDUSCON), São Paulo, Brazil, 2018, p. 298–304. DOI:10.1109/INDUSCON.2018.8627215.

[25] Ibanez FM, Echeverria JM, Astigarraga D, et al. Soft-switching forward DC-DC converter using a continuous current mode for electric vehicle applications. IET Power Electron. 10 2015;8(10):1978–1986. DOI:10.1049/iet-pel.2014.0581.

[26] Ravi Kishore KV, Brahmendra N, Sivaneasan B, et al. An APWM soft switched DC-DC converter for PV and EV. 2014 IEEE 40th Photovoltaic Specialist Conference (PVSC), Denver, CO, 2014, p. 3707–3712. doi:10.1109/PVSC.2014.6924911.

[27] Serna-Garcés SI, Montoya DG, Ramos-Paja CA. Control of a charger/discharger DC/DC converter with improved disturbance rejection for bus regulation. Energ MDPI Open Access J. 2018;11(3):1–30.

[28] Qu KQ, Niu QQ, Yang C, et al., Battery charge-discharge control strategy based on the single Z-source three-level SVPWM inverter. 2013 IEEE International Conference on Applied Superconductivity and Electromagnetic Devices, Beijing, 2013, p. 30–33.

[29] de Melo HN, Trovão JPF, Pereirinha PG, et al. A controllable bidirectional battery charger for electric vehicles with vehicle-to-grid capability. IEEE Trans Veh Technol. Jan 2018;67(1):114–123. doi:10.1109/TVT.2017.2774189.